Lab on a Chip

This is an *Accepted Manuscript*, which has been through the Royal Society of Chemistry peer review process and has been accepted for publication.

Accepted Manuscripts are published online shortly after acceptance, before technical editing, formatting and proof reading. Using this free service, authors can make their results available to the community, in citable form, before we publish the edited article. We will replace this *Accepted Manuscript* with the edited and formatted *Advance Article* as soon as it is available.

You can find more information about *Accepted Manuscripts* in the **Information for Authors**.

ARTICLE TYPE

A multi-channel device for high-density target-selective stimulation and long-term monitoring of cells and subcellular features in *C. elegans*

Hyewon Lee,‡[a] Shin Ae Kim,‡[a] Sean Coakley,[c] Paula Mugno,[c] Marc Hammarlund,[d] Massimo A. Hilliard,[c] and Hang Lu*[a,b]

Selective cell ablation can be used to identify neuronal functions in multicellular model organisms such as *Caenorhabditis elegans*. The optogenetic tool KillerRed facilitates selective ablation by enabling light-activated damage of cell or subcellular components in a temporally and spatially precise manner.
10 However, the use of KillerRed requires stimulating (5 min-1 hr), culturing (~24 hrs) and imaging (often repeatedly) a large number of individual animals. Current manual manipulation methods are limited by their time-consuming, labor-intensive nature, and their usage of anesthetics. To facilitate large-scale selective ablation, culturing, and repetitive imaging, we developed a densely-packed multi-channel device and used it to perform high-throughput neuronal ablation on KillerRed-expressing animals. The ability to
15 load worms in identical locations with high loading efficiency allows us to ablate selected neurons in multiple worms simultaneously. Our device also enables continuous observation of aminals for 24 hrs following KillerRed activation, and allows the animals to be recovered for behavioural assays. We expect this multi-channel device to facilitate a broad range of long-term imaging and selective illumination experiments in neuroscience.

Introduction

20 One goal of neuroscience is to identify how neurons and neural circuits regulate physiological outcomes, such as animal behaviour, memory, and learning.[1, 2] Many neurodegenerative conditions including Parkinson's, Alzheimer's, and Huntington's
25 diseases are associated with neuronal malfunction or damage.[3] The small nematode *Caenorhabditis elegans* (*C. elegans)* has been widely utilized for studies of neuronal function because of its simplicity, well-characterized neural connectome, ease of genetics, and its transparency, which is highly advantageous for
30 fluorescence imaging as well as optical manipulation.[4]

One way to interrogate the function of a specific neuron is to kill it and then analyze the phenotypical and physiological consequences for circuit function and animal behavior.[5, 6] Laser ablation has been widely adopted as the technique of choice to
35 kill individual neurons, as it provides a very precise, rapid and selective damage. Recently, a new optogenetic technique using a genetically-encoded photosensitizer was introduced to facilitate neuronal ablation.[7-12] The genetically-encoded photosensitizer, KillerRed (KR), is activated upon exposure to green light (540-
40 590 nm) producing reactive oxygen species (ROS), which kills the cell without secondary damage to neighboring cells and tissues.[7-11] It takes about 18-24 hrs after illumination to observe morphological damages in ablated neurons. Unlike laser ablation, KR can be activated with wide field illumination, and thus

45 multiple neurons in multiple animals can be ablated simultaneously.

To perform large-scale experiments in which circuit function, neuronal morphology, or animal behavior is characterized after KillerRed ablation, high-throughput selective stimulation, long-
50 term culturing, and parallel imaging are desired. However, traditional manual handling methods are time-consuming because they require the sequential manipulation of individual animals. Typically, each animal is placed onto an agar pad on a glass slide for ablation, moved to a bacterial lawn for culture (~24 hrs),
55 transferred back to a microscope slide for observation, and/or recovered from the slide for physiological characterization (e.g. behavioral tests). This repetitive and labor-intensive process decreases experimental throughput and makes it difficult to track the time-dependent changes of individual animals. In addition,
60 the immobilization process often involves anesthetics, which can affect developmental or regenerative processes.

To facilitate manipulation, many microfluidic devices have been designed for stimulating and imaging *C. elegans*.[13-23] Even though these microfluidic devices have superior abilities to
65 handle animals compared to manual methods, most of them consist of a single trapping channel. Such single-channel methods are incompatible with the potential to study multiple worms in parallel using KillerRed. Additionally, the fabrication processes and operations of several of these devices are relatively
70 complex due to active control elements on- or off-chip.

Multi-channel devices can increase the throughput of imaging *C. elegans*.[23-27] Hulme *et al*. created a 128 channel device to trap and image animals[24] and applied it (16 channel-version) to track the changes in body size and locomotion for entire adult life spans.[26] Although the process of loading *C. elegans* is very simple and fast, the channels of this device are not closely packed and worms are not loaded in identical locations. Thus, it is difficult to have multiple worms in a field of view for high-throughput stimulation and imaging. Moreover, while the tapering channel enables immobilizing animals for imaging at high resolution, the clasped features restrict food and chemical delivery to the worms while they are in the channel. This type of design, therefore, is unsuitable for optogenetic ablation and imaging.

To facilitate the sequential procedures of irradiation and repeated imaging of a large number of animals in parallel with continuous delivery of bacteria, we have developed a multi-channel microdevice for simple and rapid loading, trapping, stimulating, and imaging worms. The design advantage of the microfluidic device we developed are as follows: (1) trapping channels are densely packed allowing multiple animals to be stimulated and imaged simultaneously, enabling high-throughput analysis; (2) the device does not include any active components, and thus its operation is simple and does not require any expensive and complex external components; (3) chemicals, media, and bacteria can be easily delivered in a controlled manner, which is feasible for long-term observations; (4) it is easy to recover worms from the device to investigate their physiological outcomes regulated by target neuron activities; (5) the device operation is robust with negligible possibility of clogging since the size of main channel is much larger than the width of *C. elegans*. Furthermore, the device is not limited to use in optical surgery, and can be applied to many applications involving imaging and stimulating multiple *C. elegans* animals.

Materials and methods

Fabrication of devices

All microdevices were fabricated in polydimethylsiloxane (PDMS) (Dow Corning Sylgard 184, Midland, MI) by soft lithography.[28] The master molds were fabricated with a negative photoresist, SU8-2025 (Microchem, Newton, MA) by UV photolithographic processes. Before micromolding process, the surfaces of 45 µm-thick patterned wafers were treated with tridecafluoro-1,1,2,2-tetrahydrooctyl-1-trichlorosilane vapor (United Chemical Technologies, Bristol, PA) to allow release of PDMS from the masters. To obtain ~1 mm-thick layer, a PDMS mixture of A and B in 20:1 ratio was poured on the mold after removing air bubbles, and then partially cured at 70 °C for 15 min. On top of the first layer, a PDMS mixture in 10:1 was poured to obtain ~5 mm-thick second layer for mechanical integrity.[25] After fully curing the mold at 70 °C for 2 hrs, the whole PDMS layer was peeled off and devices were cut into shape. For fluidic connections, two holes (one inlet and one outlet) in individual devices were punched with 19 gauge needles (McMaster-Carr, Elmhurst, IL). Finally, all devices were bonded onto either a slide or cover glass by plasma bonding.

KillerRed-expressed *C. elegans* strain

We used a KillerRed (KR)-expressing transgenic worm: *zdIs5(Pmec-4::GFP)*, *vdEx405[Pmec-4::KR; odr-1::DsRED2]*.[10] All worms were fed with *Escherichia coli* (*E. coli*) OP50 on culturing agar plates and maintained at 20 ℃ based on standard culture conditions.[29] Hermaphrodite worms were synchronized to L4-stage before being loaded worms in the microfluidic device.

System operation and bacteria preparation

For each experiment, the microfluidic device was filled with M9 solution to remove air bubbles. Then, animals were delivered with M9 solution into the device at a flow rate of 2.5-3.5 ml/hr using a syringe pump. For feeding *C. elegans*, OP50 bacteria were cultured at 37 ^{0}C for 16 hrs shaking at ~200 rpm. To inactivate the bacteria, these cultures were spiked with Streptomycin (50 µl/ml final concentration). After spinning down the bottles at 4500rpm in a refrigerated centrifuge set at 4 ^{0}C for 20 min, supernatant was discarded and pellet was resuspended with a mixture of S-basal, Streptomycin (50 µg/ml), and Carbenicillin (50 µg/ml), to reach OD_{600}=10. The mixture including bacteria was flowed into the device in 2-3 ml/hr usually for a day. To recover animals from the device and characterize the physiological outcomes, M9 solution was introduced from the outlet (backflow) at a flow rate of 5~10 ml/hr and the animals were collected from the inlet of the device.

Microscopic setup for optical ablation and imaging cells

Two different types of microscopic systems were used for optical ablation. High-throughput ablation was performed with whole field illumination on a fluorescence dissecting scope (Leica, MZ16F) with 2x objective for 2 hrs with intensity of ~ 1 mW/mm^2. To kill the target cells by KR activation, green light was illuminated for an hour. The green light was filtered with TXR filter (green light: 560/40 nm).

For the selective optical ablation, a modified LCD projector system was employed.[30] The green colour of the LCD projector (Hitachi, CP-X605) was modified with a green filter (568/50 nm band-pass) and emission lights were measured with Hamamatsu EM-CCD camera (512 x 512 pixels) on a fluorescence scope (Leica DMIRB). Two objectives (4x and 10x) were used for selective optical ablation. The intensity were 1.6 mW/mm^2 for 4x and 6 mW/mm^2 for 10x, respectively. For selective illumination on multiple target regions, a LabVIEW program was developed to create and control multiple regions of interests (ROIs). Green light was illuminated on the selected ROIs for an hour and blue light was applied to measure the change of target GFP signals 24 hrs after illumination. The GFP signal was monitored with 4x objective for cell body observation and 20x objective for cell body and axon observation.

Computational Fluid Dynamics

To characterize the fluid dynamics in the device according to the channel geometry, a three-dimensional fluid flow model was
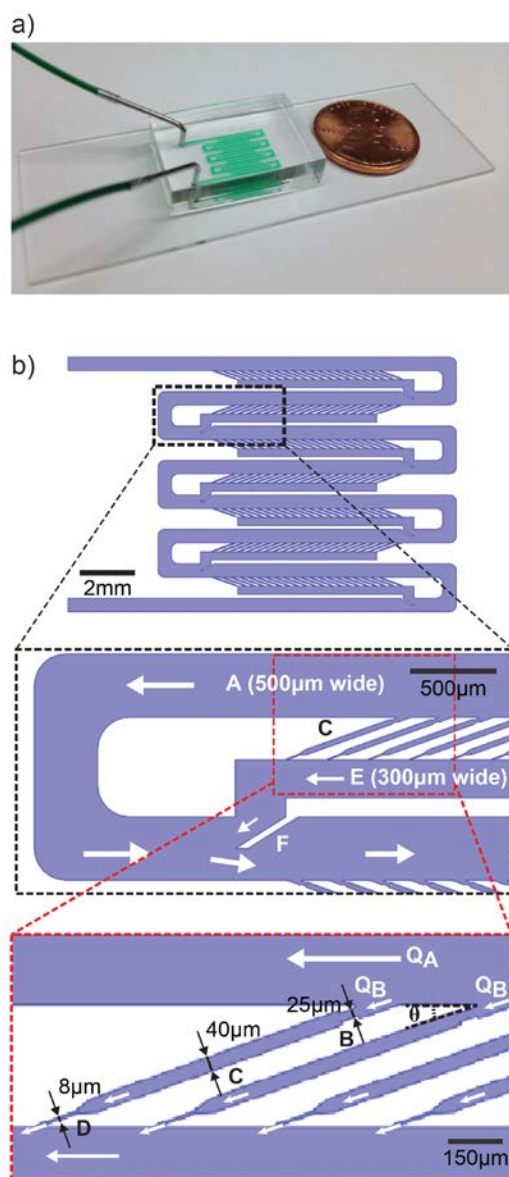
Fig. 1 a) Optical micrograph of the high-density array device. The channels were filled with colored dye for visualization. b) Schematics of the multi-channel device showing the array of 140 trapping channels
5 connected to the serpentine channel. Zoomed in views of the boxed region show the microfluidic components that enable efficient single-worm loading and continuous media delivery: A, serpentine channel; B, inlet of trapping channel; C, trapping channel for imaging individual animals; D, restriction channels; E, resistance channels; F, slanted
10 protrusion for fast recovery. White arrows represent the direction of flow which can carry worms and chemicals; specifically, Q_A represents stream flowing along the serpentine channel and Q_B indicates a steam into the trapping channel.

developed using the Computational Fluid Dynamics (CFD)
15 module of the finite element modelling software COMSOL (Stockholm, Sweden). To simplify the numerical simulations, 3 x 3 or 20 x 3 array formats were used. Incompressible steady-state Navier-Stokes equations were solved to obtain the velocity profiles. Inlet pressure was set to obtain a volumetric flow rate
20 equal to the measured value, and outlet pressure was fixed at atmospheric pressure. In the simulation, fluid density was set to 1000 kg/m^3 and dynamic viscosity was 8.90 x 10-4 Pa·s based on

the properties of water at room temperature.

Behavior assay

25 To perform the classical mechanosensory behavior assay, ablated or non-ablated control animals were placed on smooth agar testing plates one day after illumination. The testing plate was a standard agar plate prepared without OP50 bacteria. An eyelash was used to deliver gentle touch to the anterior (just behind the
30 pharynx) and posterior (just anterior to the anus) body regions,[31-33] which in wild-type animals trigger backward and forward locomotion, respectively.

Results and discussion

Design of microfluidic device

35 In order to stimulate and image a large number of animals in a high-throughput manner, we developed a simple high-density multi-channel microdevice (Fig. 1). This one-layer PDMS device includes 140 densely-packed individual channels in a 20 (column) x 7 (row) format to trap worms; it also allows for
40 stimulating and imaging worms over time. Fluid enters all trapping channels from a single serpentine channel (A, 500 μm wide), which carries worms and media throughout the device from the inlet to the outlet (Fig. 1b). The 40 μm wide trapping channels (C) fit closely with the size of young adults, which
45 allows selective isolation of animals of the same size for stimulation and imaging to monitor neuronal morphology and damage. We minimized the space between neighbouring trapping channels (~70 μm in a column) so that we achieved a density of 2.42 traps/mm^2, which is ~4 times higher than what has
50 been previously developed.[24] With 10x magnification, 6-7 trapping channels can be illuminated using a multi-channel device, compared to ~1 channel that can be visualized using previous devices.

Each trapping channel includes novel components to
55 efficiently load and confine single animals to trapping channels, and deliver chemicals uniformly without active component controls (valves) (Fig. 1b). At the outlet of each trapping channel, an 8-μm wide restriction channel (D) prevents worms from escaping, but 45-μm thick channel height enables
60 continuous flow to deliver chemicals. Additionally, continuous flow across the restriction channel is fast enough to draw worms to the end of trapping channels, facilitating positioning of the animals in relatively identical locations. Another key feature is the 300 μm wide resistance channels (E) positioned between the
65 trapping and serpentine channels, which are important for pressure balance and keeping the loaded animals in place. To achieve long-term (>10 hrs) monitoring target worms, we designed the inlet of trapping channel to be small enough to prevent worms from escaping (B). Specifically, we engineered
70 the inlet to be 25 μm wide to balance between maximizing loading efficiency and minimizing escaping of *C. elegans*.
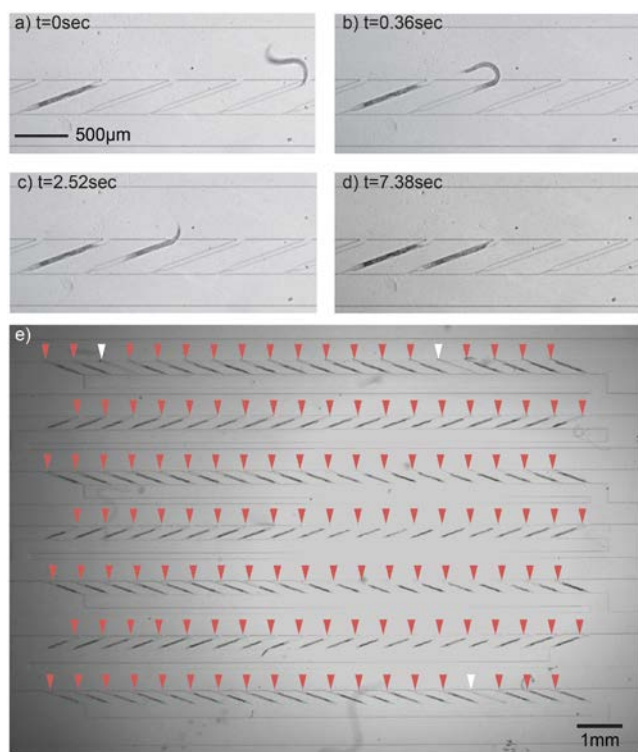
Fig. 2 *C. elegans* loading in the trapping channels. a)-d) Sequential images showing single-worm trapping in a channel in a few seconds. e) Micrograph of an entire multichannel device loaded with *C. elegans* (97.7% occupancy). Red triangles point at individual traps successfully loaded with single worms; white triangles at empty traps.

Simple and efficient trapping mechanism

The fluidic design of the chip enables rapid and efficient worm loading without the need of any active elements on the device; thus, the device operation is very simple and does not require any complex off-chip components. To minimize the variations in flow through the trapping channels and possibility of clogging, most of the fluid is engineered to travel along the serpentine channel; the small but significant enough flow across each trapping channel drags worms into the individual channels within a few seconds (Fig. 2a-d). On average, filling most of the loading channels on each chip takes less than 30 min and loading efficiency is generally higher than 80% (Fig. 2e and Supplementary video 1). It is important to note that because of active locomotion, it is not practically possible to load with 100% efficiency, i.e. the geometrical constraint cannot necessarily prevent animals from escaping. Despite this negligible limitation, we can achieve relatively high occupancy, which makes it possible to apply homogeneous optical and/ or chemical stimulation on densely-packed multiple animals in parallel. Finally, the regular array of animal facilitates repeated characterization of specific cellular or subcellular phenotypes.

### Loading efficiency depending on design geometry

Geometries were optimized in order to efficiently trap a single animal per trapping channel, and thus to achieve overall high occupancy in array microdevices. Specifically, we empirically determined the optimal angle between the trapping channel and the serpentine channel (θ) (Fig. 1b) by varying θ from 10^0 to 90^0 (Fig. 3a). We observed that small angles (e.g. 10^0 and 20^0 as

shown in the data) show superior loading efficiency. In a
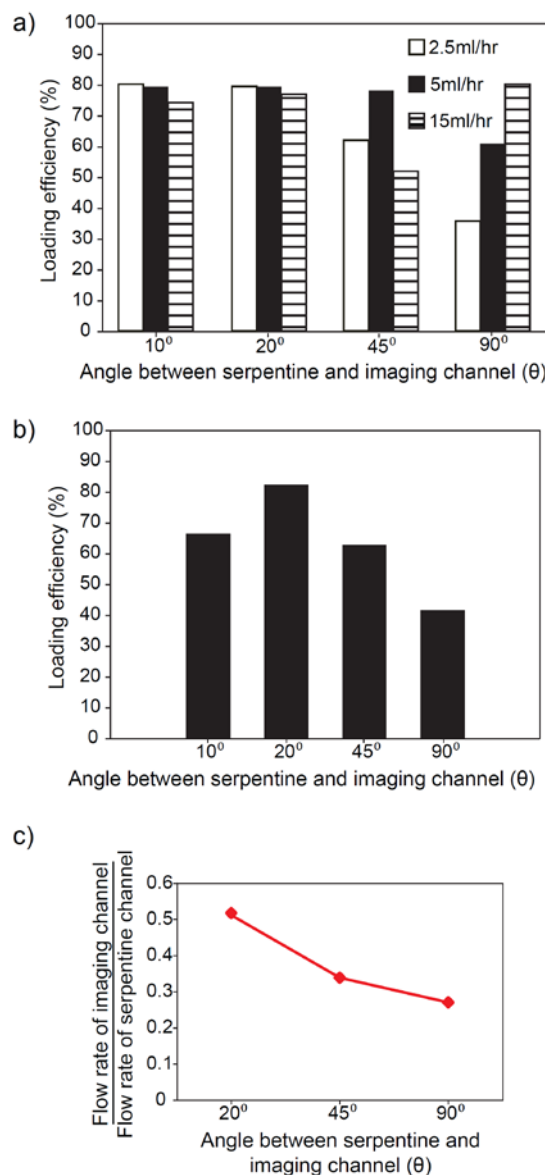
Fig. 3 Loading efficiency optimized with channel geometry, focusing on the angle between the trapping channel and the serpentine channel (θ). a) The bar graph showing the channel occupancy as a function of channel angle and flow rate. b) The graph representing the loading efficiency of *C. elegans* with 1mM tetramisole to remove worms' mobility. Loading efficiency in each group was analyzed based on two individual experiments. c) The plot of the flow ratio between serpentine and imaging channel at different angles based on COMSOL simulation.

previously published work[25], the angle (θ) is optimized as 20^0 because worms need to bend their body significantly to enter the channels if angles are too large. However, loading efficiency still depends on θ, even after immobilizing the animals with the cholinergic agonist paralyzing agent, tetramisole (Fig. 3b). We hypothesized that the balance between a stream flowing along the serpentine channel (Q_A) and a steam directing the worms into the trapping
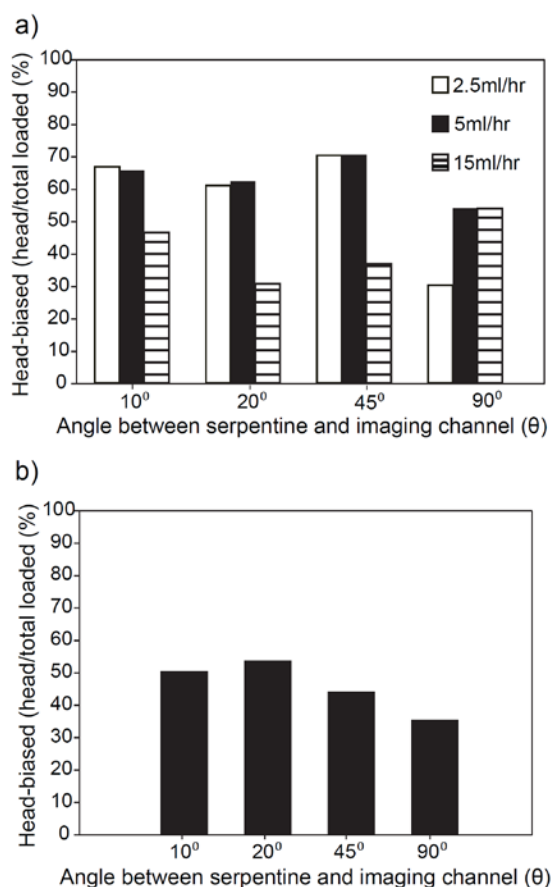
Fig. 4 The orientation of loaded worms depending on flow rates, the mobility of animals, and angles between the trapping channel and the serpentine channel (θ). The bar graphs show the head-bias of trapped animals a) without and b) with 1 mM tetramisole. Head-biased ratio in each group was analyzed based on two individual experiments.

channel (Q_B) affects the loading efficiency (Fig. 1b). To validate this idea, we characterized the flow ratio (Q_A/Q_B) based on fluid dynamics model (COMSOL) (Fig. 3c). We found that the more slanted the imaging channel, the higher the ratio of flow rates, which correlates with higher loading efficiency. The analyzed data suggest that small angles are preferred for high loading efficiency, due to a better flow rate balance as well as *C. elegans* movement.

In contrast, the head-tail orientation of the loaded worms depends more on the worm's locomotion ability and the overall flow rates (Fig. 4a, b). Head-bias is important for housing worms for a long time in the trapping channels because animals oriented tail-first tend to escape more easily. In addition, relatively uniform head-tail orientation reduces the complexity of selective illumination, as cells of interest can be easily identified without having to scan through the entire worm. If worms are consistently oriented head-first in the channels, we can roughly target the neurons of interest based on channel locations. Thus, to maximize the head-bias loading efficiency, the flow rate was optimized as 2.5-5ml/hr, with a preferred channel angle of 20^0.

Controlled delivery of chemicals, media, and bacteria

One of the advantages of this microfluidic platform is the ease of delivery of chemical and bacteria. Since worms are slightly smaller than the channel height, continuous flow was maintained through the trapping channel and confirmed using a soluble dye (data not shown). A continuous delivery is essential for bacteria supply on chip to avoid starvation, for supply of chemicals, and to image individual worms as eggs are laid because it removes newly-hatched progeny through the narrow restriction channels. To verify the successful food delivery to trapped worms, we flowed suspensions of 1.21 μm-diameter fluorescent beads. From this test, we observed beads being ingested and accumulating inside *C. elegans* body, which implies that trapped worms can easily consume the bacteria delivered (data not shown). In this experiment, we also observed regular pharyngeal pumping rates (Supplementary video 2) as well as a normal number of eggs laid after one-day culturing in the device. In contrast, animals cultured without food shows noticeably decreased pumping rate (Supplementary video 3). Pharyngeal pumping and egg-laying are well correlated with the animals sensing the presence of food, strongly indicating the animals are feeding properly.[34] We showed that the delivery of bacteria enables culturing animals in the channels for more than a day; this is beneficial in observing optical ablation, or other long-term imaging in high-throughput since worms are not required to be transferred from observation agar pad to bacterial lawn for maintenance and subsequent analysis.[35-38]

Ease of recovery without damaging animals

To analyze the physiological changes and investigate the function of specific neurons, irradiated animals need to be recovered. With this device, recovery is easily achieved by applying flow in the reverse direction. This is further facilitated by the slanted protrusion (F) we engineered at the end of each resistance channel (Fig. 1b); it prevents animals from swimming to a resistance channel, instead directing them through the serpentine channel (Fig. 5a). In the absence of the slanted protrusion, the animals can become re-trapped in the resistance channel during recovery (Fig. 5b, c). In such an event, recovery would become difficult, given that application of flow in the reverse direction will not be sufficient for the animals to pass through the narrow restriction channel that connects the resistance and serpentine channels (Fig. 1b and Fig. 5c). One possible solution could be the application of repetitive cycles of forward and reverse flow; however, this is very time-consuming. Using the slanted wall, we successfully recovered over 90% of trapped animals, which is more than twice of recovery rate without this feature (Fig. 5d).

For efficient recovery of animals, the balance of flows needs to be considered. Indeed, to inhibit worms from becoming retrapped in the resistance channel, most flow needs to

ARTICLE TYPE
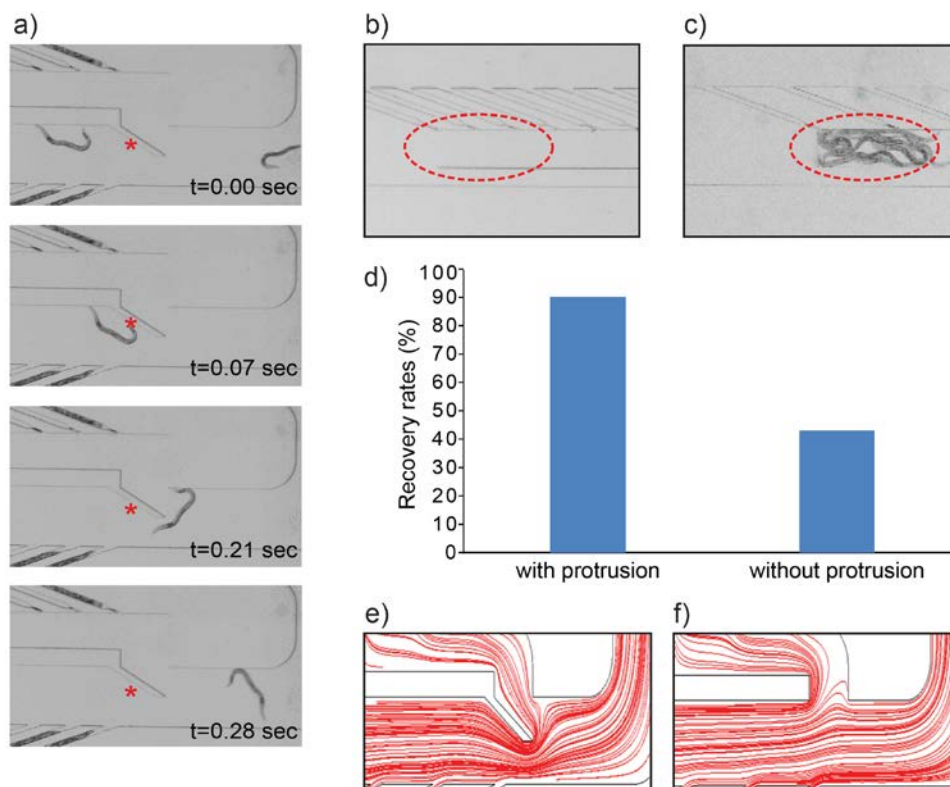
Fig. 5 The slanted protrusion enables high-throughput recovery of animals. a) Sequential images showing the efficient recovery of animals. Worms are prevented from swimming into resistance channel while traveling along the serpentine channel. Red star indicate the protrusion feature. b) Representative image of empty resistance channel showing the successful recovery due to protrusion. c) Optical photograph showing the animals re-trapped to the resistance channel after recovery in the case of no slanted protrusion. d) The bar graph showing the comparison of recovery rates with and without slanted wall. Recovery rate in each group was analyzed based on two individual experiments. e) and f) plots showing the flow stream lines e) with and f) without protrusion wall using COMSOL simulation.

travel through the serpentine channel, but some significant flow is still required in the resistance channel to push worms out of the trapping channels. The COMSOL simulation showed that the slanted wall changes the flow streams, but still allowing enough flow to go into the resistance channels (Fig. 5e, f). Overall, we found that worms could be recovered successfully within a few minutes from devices containing the slanted wall protrusion feature.

Parallel optical ablation of trapped worms

We showed that multi-channel device can successfully trap single animals with high loading efficiency (Fig. 2 and Fig. 3a). The high trapping density of our microdevice should allow for high-throughput cell ablation of *C. elegans*. We tested this method using the optical ablation tool KillerRed.[10] We used wild-type nematodes expressing KR in the mechanosensory neurons ALM (left and right) and PLM (left and right) (Fig. 6). Optical ablation with KR exploits the ability of ROS to damage target cells when green light activates KR.[8, 9] To assess the viability of target cells

before and after ablation, we used GFP co-expressed in the same cells. Fig. 6 shows GFP in ALMs and PLMs before irradiation and 24 hrs after KR activation (one hour irradiation). We found following KR activation, GFP of mechanosensory neurons vanished in the whole exposure area (Fig. 6b).   Without illumination, all neurons were intact and presented no damages when inspected after 24 hrs (Fig. 7c). By illuminating animals for 2 hrs at 2x magnification, we successfully ablated all KR-expressed neurons in the whole multi-channel device.   In principle, we should be able to ablate target cells in 140 worms at once, if all trapping channels
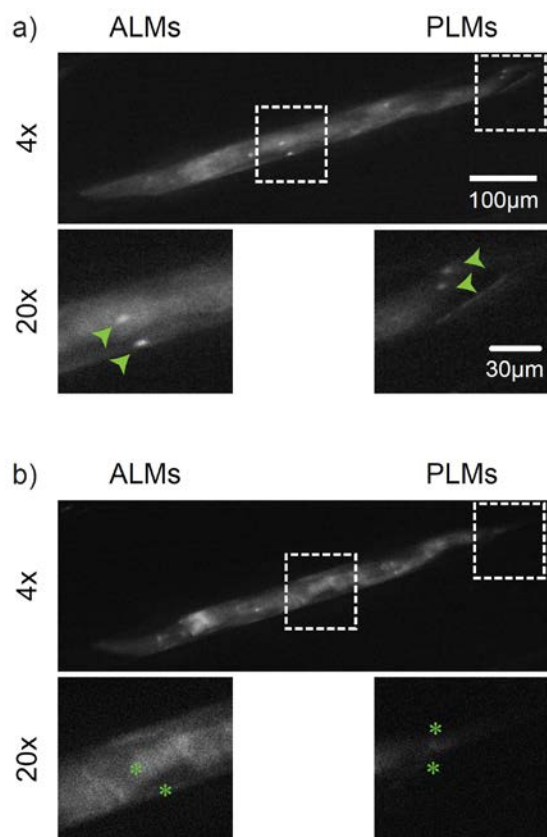
Fig. 6 Fluorescent images of ablation on mechanosensory neurons of *C. elegans* in the device. The zoom-in views (20x) of each boxed region showing GFP signals of ALMs and PLMs a) before illumination and b)
5 24 hrs after illumination. Green arrowheads = undamaged neurons, asterisks = putative position if the same neurons were alive.

are occupied with KR-expressing animals. Although in a manual experiment on agar plates we can also illuminate and ablate all KR- expressing cells in 30-50 animals at the same time, it is very
10 difficult to identify and track individual animals and measure their phenotypic changes over time after optical activation. With this newly developed chip, not only can we ablate but also monitor individual degeneration processes in parallel. Moreover, unlike manual methods such as laser ablation for selected cell-
15 killing, we are able to eliminate the need of anaesthetics, which can be disruptive to developmental and regenerative processes.

Simultaneous selective ablation of target neurons and long-term monitoring

An important advantage of the multi-channel microfluidic
20 platform is the ability to place multiple worms in identical positions within a small space. Because of the trapping channels

and continuous flow through the restriction channels, worms are positioned in predictable locations, which enable fast selection of a region of interest (ROI) for selective ablation, without the time-
25 consuming pre-imaging process to identify locations of cells. To create ROIs, we used a customized LCD projector system similar to that we previously developed in Stirman *et al*.[30] Fig. 7a shows results of selective illumination on PLMs (marked with green arrow heads) of a trapped worm. We observed the target-cell
30 death 24 hrs after illumination; in contrast, unilluminated ALMs (marked with white arrow heads) in the same worms were phenotypically unaffected.

To be able to monitor cell death over time (~24 hrs), we also characterized the ability of our microfluidic chip to culture
35 animals and continuously deliver bacteria. Even during illumination to activate KR, especially when it takes more than 30 min, it is important to allow *C. elegans* to feed to minimize side effects. This is an unmet need in microfluidics engineering because previously developed platforms do not allow sufficient
40 immobilization for region-specific targeting while allowing for feeding. In our experiment, worms were fed during and after illumination and can survive more than a day on chip. We measured and compared the relative pharyngeal pumping rate with and without food delivery (Fig. 7b). While the pharyngeal
45 pumping rate with food is comparable to that of culturing plate condition (control), without-food condition shows dramatically decreased pumping rate. This suggests that animals are feeding properly on the multi-channel device, providing the opportunity to increase the experimental throughput by eliminating repeated
50 worm-transfer between culturing plates and ablation/observation pads.

Next, to observe the phenotypic changes, we collected time-lapse images hourly after the PLM illumination. Fig. 7c shows the results of time-dependent phenotypic changes for 19 hrs on
55 two sets of different animals: one with PLM illumination and the other with no illumination. Interestingly, we observed different rates of cell deaths in a single PLM pair; one of the GFP signals disappeared after 6 hrs, while the contralateral one after 9 hrs (Fig. 7c upper row, right worm). Additionally, we also observed
60 different rate of degeneration between soma and axon. In contrast, control worms maintained GFP signals in axons and somas for 19 hrs. These results demonstrate that our device is capable of analyzing dynamic processes with subcellular resolution. Thus, this microfluidic platform can be applied to
65 monitor degenerative or regenerative progress on subcellular level *in vivo* in multiple animals, which is useful in aging and neurodegenerative disease studies.

Post-illumination recovery and behavior assay

ARTICLE TYPE
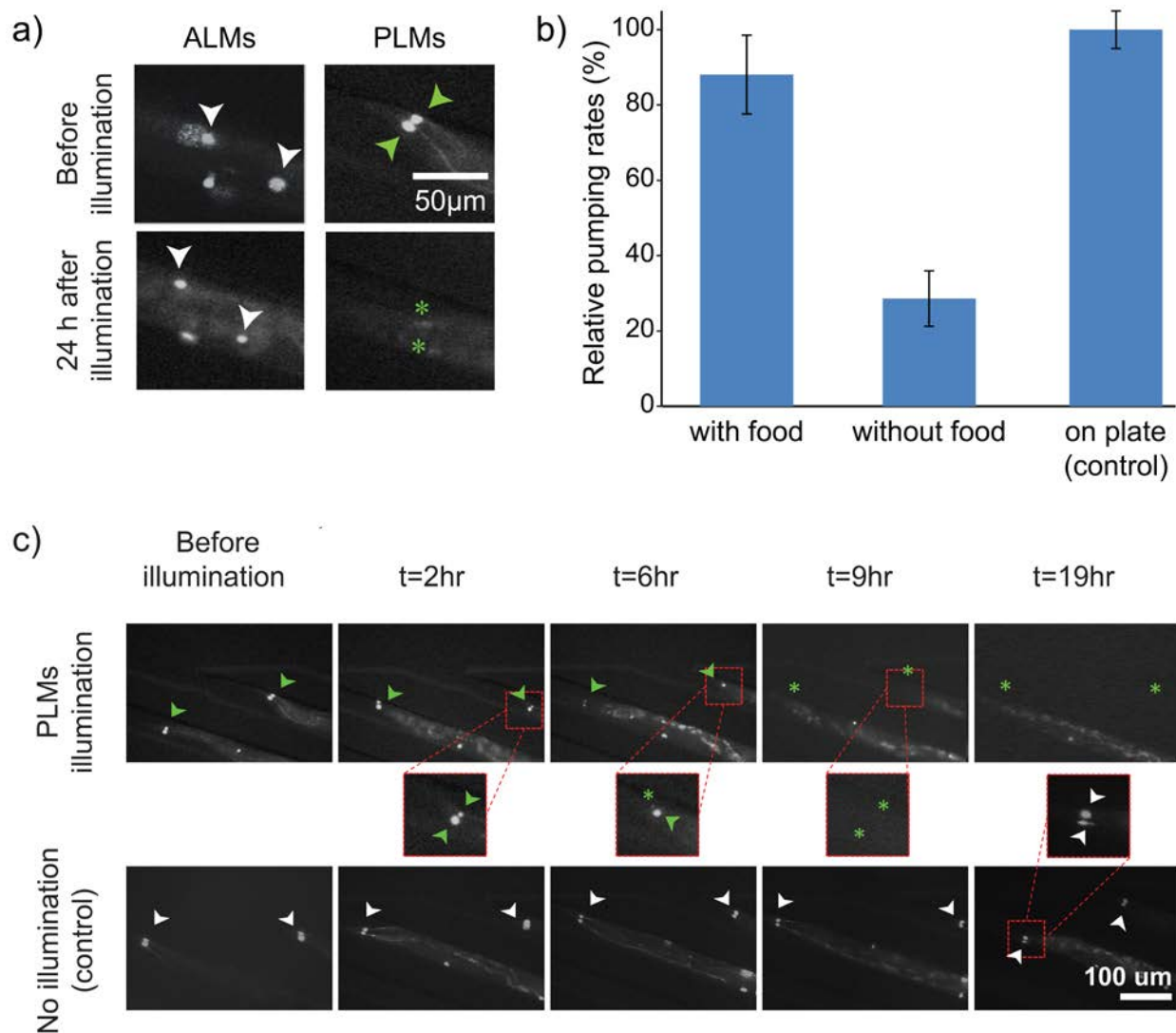
Fig. 7 Selective neuronal ablation and long-term monitoring of multiple animals on the device. a) Fluorescent images of ALMs and PLMs of a single animal showing selective PLMs ablation. PLMs were illuminated for an hour with green light and imaged after one-day culture on the device. Green arrowheads and asterisks mark intact and vanished GFP signals on PLMs respectively; white arrowheads indicate control ALMs which has no changes. b)
5 Relative pharyngeal pumping rates of worms with and without food (OP50 bacterial solution, OD600 = 10) on chip, normalized to animals on standard agar plate with bacteria lawns (control). The pumping rates were averaged of three individual measurements. Error bars represent standard error of means, n=5 for each group. c) Time-lapse images of GFP signals of PLMs for 19 hrs after 1hr PLMs-selective illumination (upper) and without illumination (control, lower). The GFP intensity of illuminated PLMs decreases as a function of time, while without illumination all PLM signals have no critical changes. Arrowheads point PLM bodies and asterisks indicate vanished GFP signals on PLM bodies.

10 We have shown that animals can easily be recovered with high efficiency without critical damage or worm loss in this newly designed device (Fig. 5). It is essential to analyze the physiological outcomes (e.g. behavior) of recovered animals for investigating the function of ablated cells. It has been shown that
15 *C. elegans* mechanosensory neurons are responsible for detecting gentle touches (light-touch) in the anterior (ALMs) and posterior (PLMs) of the animal's body[31, 33], causing worms to move backwards and forwards, respectively (Supplementary Fig. 1a). As a proof of concept, we performed the light-touch assay on
20 normal (Supplementary video 4) or ablated animals (Supplementary video 5, 6) to determine the functional consequences of on-chip ablation. The presence or absence of neurons was confirmed after the behavioral assays by examining the presence of GFP. As expected, we found that animals with a
25 set of either ALMs or PLMs ablated failed to respond to either

anterior or posterior body touch (Supplementary Fig. 1b-e) Animals with PLMs ablated showed halting or no accelerated forward locomotion after being touched on the posterior body, while the same worms showed normal backward locomotion after being touched anteriorly (Supplementary Fig. 1b, c and Supplementary video 5). By contrast, animals with ALMs ablated showed no backward locomotion in response to anterior body touch, while they responded normally to posterior touch (Supplementary video 6). When examined after the behaviour assay, worms insensitive to the anterior body touch did not have GFP signals in ALMs while having intact GFP signals in PLMs (Supplementary Fig. 1d, e). These results are consistent with previous findings related to the function of these neurons.[31, 33] Based on behavioral tests and GFP imaging, it is evident that illumination on KR-expressed neurons disrupts their function as well as cellular phenotypic changes. Our results also demonstrated that the device is capable of executing localized damage (in combination with KR) and long-term culturing under growing conditions, as well as allowing observations of phenotypic changes at high spatial and temporal resolution. Additionally, animals can be recovered efficiently and gently for further analysis.

Conclusions

Here we present the development of a multi-channel microfluidic device that can load, trap, and image over 100 worms at the same time. This high-density array platform enables studying and optically manipulating multiple targets without active fluidic elements. In addition, the continuous nutrient supply in the device enables both long-term imaging and irradiation. The ability of long-term monitoring in our device may be applicable to degenerative, regenerative, and developmental studies that require study of transient responses or time-lapse changes. For example, it is easy to track the cellular and subcellular response (e.g. mitochondria distribution) to ROS over time. In addition, this controlled delivery has potential benefits in the supply of chemical stimulants to record neuronal responses such as calcium imaging and drug screening. Lastly, the ability to safely recover animals from our device can be useful for continuing studies, such as functional behaviour tests. We envision that this device will facilitate many future experiments using optogenetics and functional imaging to understand how neurons develop and degenerate as animals age, how neural circuits are formed, and how they produce behaviour.

Acknowledgements

Notes and references

ª School of Chemical & Biomolecular Engineering, Georgia Institute of Technology
ᵇ Interdisciplinary Program of Bioengineering, Georgia Institute of Technology
ᶜ Queensland Brain Institute, The University of Queensland, Brisbane QLD 4072, Australia
ᵈ Department of Genetics, Program in Cellular Neuroscience, Neurodegeneration and Repair, Yale University
* 311 Ferst Dr, NW, Atlanta, GA 30332-0100, USA. Fax: +1-404-894-8473; Tel: +1-404-894-8473; E-mail: hang.lu@gatech.edu;

‡ These authors contributed equally.

1. A. C. Keene and S. Waddell, *Nature reviews. Neuroscience*, 2007, **8**, 341-354.
2. E. Z. Macosko, N. Pokala, E. H. Feinberg, S. H. Chalasani, R. A. Butcher, J. Clardy and C. I. Bargmann, *Nature*, 2009, **458**, 1171-1175.
3. K. J. De Vos, A. J. Grierson, S. Ackerley and C. C. Miller, *Annu. Rev. Neurosci.*, 2008, **31**, 151-173.
4. S. Brenner, *Genetics*, 1974, **77**, 71-94.
5. C. I. Bargmann and L. Avery, *Methods Cell Biol*, 1995, **48**, 225-250.
6. C. Fang-Yen, C. V. Gabel, A. D. Samuel, C. I. Bargmann and L. Avery, *Methods Cell Biol*, 2012, **107**, 177-206.
7. M. E. Bulina, K. A. Lukyanov, O. V. Britanova, D. Onichtchouk, S. Lukyanov and D. M. Chudakov, *Nature Protocols*, 2006, **1**, 947-953.
8. T. Shibuya and Y. Tsujimoto, *Journal of Photochemistry and Photobiology B: Biology*, 2012.
9. M. E. Bulina, D. M. Chudakov, O. V. Britanova, Y. G. Yanushevich, D. B. Staroverov, T. V. Chepurnykh, E. M. Merzlyak, M. A. Shkrob, S. Lukyanov and K. A. Lukyanov, *Nature biotechnology*, 2006, **24**, 95-99.
10. D. C. Williams, R. E. Bejjani, P. M. Ramirez, S. Coakley, S. A. Kim, H. Lee, Q. Wen, A. Samuel, H. Lu, M. A. Hilliard and M. Hammarlund, *Cell Reports*, 2013, **5**, 553-563.
11. J. Kobayashi, H. Shidara, Y. Morisawa, M. Kawakami, Y. Tanahashi, K. Hotta and K. Oka, *Neuroscience letters*, 2013.
12. Y. B. Qi, E. J. Garren, X. Shu, R. Y. Tsien and Y. Jin, *Proceedings of the National Academy of Sciences*, 2012, **109**, 7499-7504.
13. S. X. Guo, F. Bourgeois, T. Chokshi, N. J. Durr, M. A. Hilliard, N. Chronis and A. Ben-Yakar, *Nature methods*, 2008, **5**, 531-533.
14. T. V. Chokshi, D. Bazopoulou and N. Chronis, *Lab on a chip*, 2010, **10**, 2758-2763.
15. H. Lee, M. M. Crane, Y. Zhang and H. Lu, *Integrative biology : quantitative biosciences from nano to macro*, 2012.
16. M. M. Crane, K. Chung and H. Lu, *Lab on a chip*, 2009, **9**, 38-40.
17. K. Chung, M. M. Crane and H. Lu, *Nature methods*, 2008, **5**, 637-643.
18. K. Chung and H. Lu, *Lab on a chip*, 2009, **9**, 2764-2766.
19. C. B. Rohde, F. Zeng, R. Gonzalez-Rubio, M. Angel and M. F. Yanik, *Proceedings of the National Academy of Sciences*, 2007, **104**, 13891-13895.
20. N. Chronis, M. Zimmer and C. I. Bargmann, *Nature methods*, 2007, **4**, 727-731.
21. F. Zeng, C. B. Rohde and M. F. Yanik, *Lab on a chip*, 2008, **8**, 653-656.
22. M. M. Crane, J. N. Stirman, C. Y. Ou, P. T. Kurshan, J. M. Rehg, K. Shen and H. Lu, *Nature methods*, 2012, **9**, 977-980.
23. J. N. Stirman, M. Brauner, A. Gottschalk and H. Lu, *Journal of neuroscience methods*, 2010, **191**, 90-93.
24. S. E. Hulme, S. S. Shevkoplyas, J. Apfeld, W. Fontana and G. M. Whitesides, *Lab on a chip*, 2007, **7**, 1515-1523.

25. K. Chung, M. Zhan, J. Srinivasan, P. W. Sternberg, E. Gong, F. C. Schroeder and H. Lu, *Lab on a chip*, 2011, **11**, 3689-3697.
26. S. E. Hulme, S. S. Shevkoplyas, A. P. McGuigan, J. Apfeld, W. Fontana and G. M. Whitesides, *Lab on a chip*, 2010, **10**, 589-597.
27. W. Shi, H. Wen, Y. Lu, Y. Shi, B. Lin and J. Qin, *Lab on a chip*, 2010, **10**, 2855-2863.
28. D. C. Duffy, J. C. McDonald, O. J. Schueller and G. M. Whitesides, *Analytical chemistry*, 1998, **70**, 4974-4984.
29. T. Stiernagle, *WormBook : the online review of C. elegans biology*, 2006, 1-11.
30. J. N. Stirman, M. M. Crane, S. J. Husson, S. Wabnig, C. Schultheis, A. Gottschalk and H. Lu, *Nature methods*, 2011, **8**, 153-158.
31. M. Chalfie, J. E. Sulston, J. G. White, E. Southgate, J. N. Thomson and S. Brenner, *The Journal of neuroscience*, 1985, **5**, 956-964.
32. M. Chatzigeorgiou, L. Grundy, K. S. Kindt, W. H. Lee, M. Driscoll and W. R. Schafer, *Journal of neurophysiology*, 2010, **104**, 3334-3344.
33. S. R. Wicks and C. H. Rankin, *The Journal of neuroscience*, 1995, **15**, 2434-2444.
34. L. Avery and H. R. Horvitz, *The Journal of experimental zoology*, 1990, **253**, 263-270.
35. Y. B. Qi, E. J. Garren, X. Shu, R. Y. Tsien and Y. Jin, *Proceedings of the National Academy of Sciences of the United States of America*, 2012, **109**, 7499-7504.
36. X. Shu, V. Lev-Ram, T. J. Deerinck, Y. Qi, E. B. Ramko, M. W. Davidson, Y. Jin, M. H. Ellisman and R. Y. Tsien, *PLoS biology*, 2011, **9**, e1001041.
37. B. Neumann, K. C. Nguyen, D. H. Hall, A. Ben-Yakar and M. A. Hilliard, *Developmental dynamics : an official publication of the American Association of Anatomists*, 2011, **240**, 1365-1372.
38. L. Kirszenblat, B. Neumann, S. Coakley and M. A. Hilliard, *Molecular biology of the cell*, 2012.

Lab on a Chip Accepted Manuscript